

Higher-order simplicial synchronization in coupled  $D$ -dimensional topological Kuramoto modelJiangsheng Wang <sup>1</sup>, Changgui Gu <sup>1,\*</sup>, Wei Zou <sup>2</sup>, Haiying Wang <sup>1</sup>, Huijie Yang <sup>1</sup>, Man Wang <sup>3</sup>, and Jürgen Kurths <sup>4,5</sup><sup>1</sup>Department of Systems Science, Business School, University of Shanghai for Science and Technology, Shanghai 200093, China<sup>2</sup>School of Mathematical Sciences, South China Normal University, Guangzhou 510631, China<sup>3</sup>School of Foreign Languages, Qingdao University, Qingdao 266071, China<sup>4</sup>Potsdam Institute for Climate Impact Research (PIK), Potsdam 14415, Germany<sup>5</sup>Department of Physics, Humboldt University Berlin, Berlin 12489, Germany

(Received 25 November 2024; accepted 26 March 2025; published 30 April 2025)

In this paper, we propose a  $D$ -dimensional topological Kuramoto model and investigate its synchronization on simplicial complexes. This model extends the higher-order Kuramoto model [Phys. Rev. Lett. **124**, 218301 (2020)] to the  $D$ -dimensional sphere, where dynamics defined on simplices of different dimensions are governed by the  $D$ -dimensional Kuramoto model. By adopting an adaptive coupling, new phenomena of phase transitions are observed. Specifically, for nodal dynamics of odd dimensions, a double discontinuous synchronization transition is observed, whereas for the Kuramoto model defined on links, a single discontinuous synchronization transition occurs. Rigorous theoretical analysis reveals that the double discontinuous transition originates from the loss of stability of the incoherent state and a saddle-node bifurcation in the parameter space. Furthermore, for the  $D$ -dimensional Kuramoto model defined on links with  $D > 2$ , synchronization is unattainable because of the inability to project dynamics onto adjacent dimensional simplices. Our findings provide insights into collective behaviors in high-dimensional spaces, such as collective defense mechanisms or social synchronization in insect swarms, mediated by higher-order signal transmission or environmental coupling.

DOI: [10.1103/PhysRevResearch.7.023103](https://doi.org/10.1103/PhysRevResearch.7.023103)

## I. INTRODUCTION

From swimming bacteria and aggregating ciliates to flocks of birds and schools of fish, communication among dynamic agents facilitates the emergence of collective behaviors across these multi-scale systems [1–6]. Evidence suggests that these communications may be controlled by the underlying dynamics. At the cellular scale, neurotransmitter transmission is controlled by glial cells [7], while local neuronal activities are affected by the dynamics of blood vessels [8,9]. In biological transport networks, flow dynamics can spontaneously generate oscillatory currents [10–12]. Notably, in quantum computations involving anyons or bosons, signals defined on links of a certain array are given significant attention [13–16]. These examples demonstrate that in addition to easily observable individual behaviors, it is also necessary to reveal hidden communication within a complex system.

Communication among individuals can be viewed as links between nodes in a complex network. In topology, links and nodes are referred to as one-dimensional and zero-dimensional simplices, respectively. They are glued together with higher-dimensional simplices to form a simplicial complex, which is believed to capture the higher-order topological

features of complex systems. Millán, Torres, and Bianconi proposed a higher-order Kuramoto model [17], which requires the Kuramoto dynamics to be defined on a simplicial complex. This model overcomes the limitation that the dynamics must be associated with the nodes in the network, and defines the dynamic variables on simplices of different dimensions, which are also called topological signals [17–22]. Based on the higher-order Kuramoto model, studies on explosive topological synchronization [20], higher-order diffusion [23,24], Dirac dynamics [25–27], and global topological synchronization [28] have emerged.

It is worth noting that for higher-order Kuramoto models, the higher order is reflected in the dynamics defined on simplicial complexes [17,29]. In this model, the state variables (phases) associated with simplices of any dimension are one-dimensional variables rather than higher-dimensional vectors. However, extending the state variables to higher-dimensional variables may be more suitable for revealing the emergent dynamics observed in various real-world systems. For example, higher-order structures are thought to be hidden in the dynamics of opinion propagation, where individual opinions in social consensus exhibit distinct high-dimensional features [30,31]. Another example is that higher-order signals play a crucial role in the collective motion of insect colonies or active colloids, where the alignment of velocity vectors is a problem widely encountered in three-dimensional space [32]. Clearly, the higher-order Kuramoto model is incapable of addressing the alignment of topological signals in high-dimensional spaces.

The  $D$ -dimensional Kuramoto model provides an ideal dynamic for introducing high-dimensional phases in the

\*Contact author: [gu\\_changgui@163.com](mailto:gu_changgui@163.com)

higher-order Kuramoto model. Olfati-Saber introduced a higher-dimensional generalization of the Kuramoto model, where the phase is defined as a  $D$ -dimensional unit vector [33]. By defining the natural rotation of individuals as a  $D$ -dimensional antisymmetric matrix, Chandra, Girvan, and Ott provided a detailed analysis of the dynamics of the  $D$ -dimensional generalized Kuramoto model with heterogeneous natural rotations [32]. In recent years, a series of fascinating works have emerged on the  $D$ -dimensional Kuramoto model and its variants [34–42].

In this paper, we propose a mathematical model to describe the topological signals governed by  $D$ -dimensional Kuramoto dynamics, which is referred to as the  $D$ -dimensional topological Kuramoto model. Building upon the higher-order Kuramoto model, this model extends the phases defined on simplicial complexes to  $D$ -dimensional vectors. The structure of the paper is as follows. In the first section, the background of this paper is introduced. In the second section, the previously studied higher-order Kuramoto model and  $D$ -dimensional Kuramoto model are presented, and the  $D$ -dimensional topological Kuramoto model is formulated. In the third section, numerical simulations are provided. In the fourth section, the framework for theoretical analysis is shown. In the last section, a summary and outlook are presented. In the Appendix, the definitions of the main concepts in the text, as well as details regarding stability analysis and self-consistent solutions for order parameters are provided.

## II. MODEL

The  $D$ -dimensional topological Kuramoto model generalizes the higher-order Kuramoto model by extending the phases defined on simplices of different dimensions to  $D$ -dimensional vectors. The schematic illustration is shown in Fig. 1, which demonstrates the relationship between our model and the existing models. Panel (a) presents the Kuramoto model, where the dynamics are defined on nodes. Panel (b) illustrates the higher-order Kuramoto model, which requires the Kuramoto dynamics to be defined on simplices of different dimensions. Panel (c) describes the  $D$ -dimensional topological Kuramoto model, where the  $D$ -dimensional Kuramoto dynamics are defined on simplices of different dimensions.

The three-dimensional (3D) Kuramoto model, as a representative of odd-dimensional Kuramoto models, has been shown to exhibit completely different phase transitions compared to even-dimensional systems in previous studies. When the Kuramoto model is extended to three dimensions, agents exhibit rotations on the surface of a three-dimensional sphere. This means that it is easier to visualize compared to those models with  $D > 3$ . The vectors rotating on the three-dimensional sphere can simulate nonlinear phenomena in processes such as ciliary beating or ferromagnetic resonance [43–47]. In this paper, the 3D Kuramoto model will be the focus of research.

### A. Higher-order Kuramoto model

The Kuramoto model is the most-widely used model for studying synchronization, which mathematical

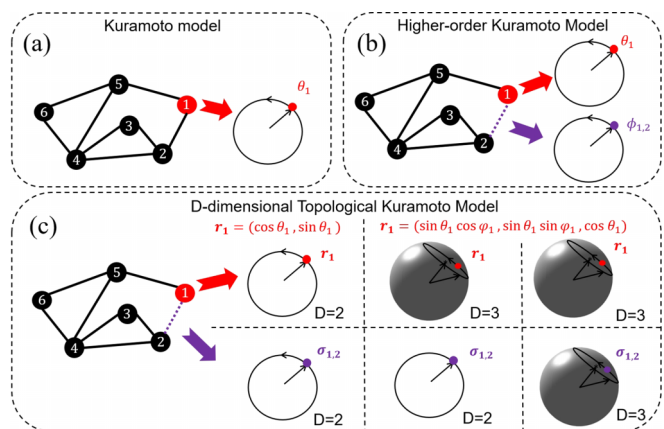


FIG. 1. Schematic illustration of the  $D$ -dimensional topological Kuramoto model. (a) The Kuramoto model in complex networks, where each node maintains its own Kuramoto dynamics with phase  $\theta_i$ . Here,  $i$  denotes the  $i$ th node. (b) The higher-order Kuramoto model in simplicial complexes, where both nodes and links (higher-dimensional simplices exist but are not shown) maintain Kuramoto dynamic variables, with phases  $\theta_i$  and  $\phi_{j,k}$ , respectively. Here,  $[j, k]$  denotes the link connecting  $j$ th node to  $k$ th node. (c) The  $D$ -dimensional topological Kuramoto model in simplicial complexes, where each node and each link maintain a  $D$ -dimensional Kuramoto dynamics, with phases  $r_i$  and  $\sigma_{j,k}$ , respectively. Taking  $r_i$  as an example, for  $D = 2$ , it is given by  $r_i = (\cos \theta_i, \sin \theta_i)$ , while for  $D = 3$ , it takes the form  $r_i = (\sin \theta_i \cos \varphi_i, \sin \theta_i \sin \varphi_i, \cos \theta_i)$ . Similarly, the  $D$ -dimensional vector  $\sigma_i$  has the same structural composition. Three cases are visualized, where agents rotate on the unit circle when  $D = 2$  and on the surface of a three-dimensional sphere when  $D = 3$ .

expression is

$$\dot{\theta}_i = \omega_i + \lambda \sum_{j=1}^N a_{ij} \sin(\theta_j - \theta_i), \quad (1)$$

where  $i = 1, 2, \dots, N$ .  $\omega_i$  is the natural frequency,  $\lambda$  is the parameter of coupling strength,  $a_{ij}$  is the element of the adjacency matrix. The dynamics are defined on nodes, and the links control the coupling relationship between nodes.

In Millán [17], by introducing the boundary map in algebraic topology, the incidence matrix  $\mathbf{B}_{[p]}$  describes the topological relationship between  $p$ -dimensional and  $(p + 1)$ -dimensional simplices. See Appendix for more details about  $\mathbf{B}_{[p]}$ . By defining the incidence matrix, Eq. (1) can be written as

$$\dot{\boldsymbol{\theta}} = \boldsymbol{\omega} - \lambda \mathbf{B}_{[1]} \sin(\mathbf{B}_{[1]}^T \boldsymbol{\theta}). \quad (2)$$

Here,  $\boldsymbol{\theta}$  is the vector of phases associated with all nodes, and its expression are  $\boldsymbol{\theta} = (\theta_1, \theta_2, \dots, \theta_{N_{[0]}})$ . Likewise,  $\boldsymbol{\omega}$  is the vector of natural frequency  $\omega_i$ . The notation  $\sin \mathbf{x}$  indicates that the sine function is applied to the elements of the matrix  $\mathbf{x}$ .

The higher-order Kuramoto model is established when the Kuramoto dynamics is set to be associated with the  $p$ -dimensional simplex. Ghorbanchian *et al.* proposed a more specific scenario, also known as the “model nodes-links”, which considers the coupling dynamics only on nodes and links (i.e., zero-dimensional and one-dimensional simplices)

[20]. The model is described as follows:

$$\begin{aligned}\dot{\theta} &= \omega - \lambda \mathbf{B}_{[1]} \sin(\mathbf{B}_{[1]}^T \theta), \\ \dot{\phi} &= \tilde{\omega} - \lambda (\mathbf{B}_{[1]}^T \sin(\mathbf{B}_{[1]} \phi) + \mathbf{B}_{[2]} \sin(\mathbf{B}_{[2]}^T \phi)).\end{aligned}\quad (3)$$

Here,  $\phi = (\phi_{l_1}, \phi_{l_2}, \dots, \phi_{l_{N_{[1]}}})$ , where  $\phi_{l_n}$  denote the phase associated with the  $n$ th link  $l_n$ .  $\tilde{\omega}$  is the vector of intrinsic frequencies  $\tilde{\omega}$  associated with each link. Equation (3) effectively captures the key characteristics of the higher-order Kuramoto model while also providing convenience for theoretical analysis. In this paper, we specifically focus on this scenario of topological signals defined on both nodes and links.

### B. $D$ -dimensional Kuramoto model

In order to mimic the more realistic situation of swarms in higher dimensions, the Kuramoto model has been generalized to high dimensions. In this framework, the motions of agents can be thought of as unit vectors rotating on the surface of a  $D$ -dimensional sphere. The  $D$ -dimensional Kuramoto model is described by

$$\dot{\mathbf{r}}_i = \mathbf{W}_i \mathbf{r}_i + \lambda \sum_{j=1}^N a_{ij} (\mathbf{r}_j - (\mathbf{r}_j \cdot \mathbf{r}_i) \mathbf{r}_i). \quad (4)$$

$\mathbf{W}_i$  and  $\mathbf{r}_i$  characterizing the natural rotation and the phase of the  $i$ th agent, respectively.  $\mathbf{W}_i$  is a real  $D \times D$  antisymmetric matrix with  $D(D-1)/2$ , and  $\mathbf{r}_i$  is a  $D$ -dimensional unit vector  $(r_{i1}, \dots, r_{ij})$  with  $j = 1, \dots, D$ .

For 3D Kuramoto model,  $\mathbf{W}_i$  is a real  $3 \times 3$  antisymmetric matrix as

$$\mathbf{W}_i = \begin{pmatrix} 0 & -\omega_{3,i} & \omega_{2,i} \\ \omega_{3,i} & 0 & -\omega_{1,i} \\ -\omega_{2,i} & \omega_{1,i} & 0 \end{pmatrix}. \quad (5)$$

The term  $\mathbf{W}_i \mathbf{r}_i$  can be represented as  $\boldsymbol{\omega}_i \times \mathbf{r}_i$ , where  $\boldsymbol{\omega}_i = (\omega_{1,i}, \omega_{2,i}, \omega_{3,i})^T$  and  $\mathbf{r}_i = (\sin \theta \cos \varphi, \sin \theta \sin \varphi, \cos \theta)^T$ . For the uncoupled dynamics, i.e.,  $\lambda = 0$ ,  $\mathbf{r}_i$  precesses around the rotation axis  $\hat{\boldsymbol{\omega}}_i = \boldsymbol{\omega}_i / |\boldsymbol{\omega}_i|$  at the rotation frequency  $\omega_i = |\boldsymbol{\omega}_i|$  along the surface of the unit sphere. Therefore the vector  $\boldsymbol{\omega}_i$  can be physically interpreted as the natural rotation of the  $i$ th uncoupled agent. For  $\lambda \neq 0$ , the norm  $\mathbf{r}_i = 1$  is always conserved because the right-hand side of Eq. (4) is orthogonal to  $\mathbf{r}_i$ .

For the model of  $D = 2$ ,  $\mathbf{W}_i$  and  $\mathbf{r}_i$  are expressed as  $\mathbf{W}_i = \begin{pmatrix} 0 & -\omega_i \\ \omega_i & 0 \end{pmatrix}$  and  $\mathbf{r}_i = (\cos \theta_i, \sin \theta_i)$ , respectively. Given that  $\mathbf{W}_i$  and  $\mathbf{r}_i$  are controlled by the unique elements  $\omega_i$  and  $\theta_i$ , respectively, it follows that Eq. (4) is equivalent to Eq. (1). In other words, the  $D$ -dimensional Kuramoto model is consistent with the classical Kuramoto model when  $D = 2$ .

The order parameter can capture the collective dynamics in a system of coupled oscillators. In the coupled  $D$ -dimensional Kuramoto model, it is defined as

$$\boldsymbol{\rho} = \frac{1}{N} \sum_{j=1}^N \mathbf{r}_j, \quad (6)$$

whose amplitude  $R = |\boldsymbol{\rho}|$  characterizes the degree of synchronization.  $R = 1$  indicates a coherent state of the system (i.e.,  $\mathbf{r}_i$  are identical), while  $R = 0$  denotes an incoherent state (i.e.,

$\mathbf{r}_i$  are uniformly distributed on the sphere). Here,  $|\cdot|$  indicates the  $L_2$  norm, ranging between 0 and 1.

### C. $D$ -dimensional topological Kuramoto model

Although the higher-order topological model and the  $D$ -dimensional Kuramoto model have been studied separately, the study of topological signals governed by the high-dimensional Kuramoto model is rare. In the study of Li [22], the topological signals are represented by a finite number of homogeneous high-dimensional oscillators. However, when the number of oscillators tends to infinity and their dynamical parameters are heterogeneous, the synchronization process of the system remains unknown.

Here, we propose the  $D$ -dimensional topological Kuramoto model, which mathematical expression is

$$\dot{\mathbf{r}} = \mathbf{F} - \lambda (\mathbf{L}_{[p]} \mathbf{r} - \mathbf{I}_N \odot (\mathbf{L}_{[p]} \mathbf{r} \mathbf{r}^T)) \mathbf{r}. \quad (7)$$

Here,  $\mathbf{F} = [\mathbf{W}_1 \mathbf{r}_1, \dots, \mathbf{W}_N \mathbf{r}_N]^T$ ,  $\mathbf{I}_N$  is a  $N \times N$  identity matrix, and  $\odot$  is Hadamard product.  $\mathbf{L}_{[p]}$  is the higher-order Laplacian, which generalizes the graph Laplacian by describing diffusion taking place on  $p$ -dimensional simplex [17]. According to the definition of  $\mathbf{L}_{[p]}$ , it can be represented by the incidence matrix  $\mathbf{B}_{[p]}$ , that is,

$$\mathbf{L}_{[p]} = \mathbf{B}_{[p]}^T \mathbf{B}_{[p]} + \mathbf{B}_{[p+1]} \mathbf{B}_{[p+1]}^T =: \mathbf{L}_{[p]}^+ + \mathbf{L}_{[p]}^-. \quad (8)$$

In Appendix A, we explain that when  $p = 0$ , Eq. (7) is equivalent to Eq. (4), and when  $D = 2$ , Eq. (7) is equivalent to Eq. (1).

Corresponding to the visual classification shown in Fig. 1(c), Table I presents three cases of topological signals associated with  $D$ -dimensional Kuramoto dynamics. For the first case, the dimensions of the Kuramoto dynamics associated with both nodes and links are  $D = 2$ , which is consistent with the expression of Eq. (3). For the second case, the dimensions of the Kuramoto dynamics associated with nodes and links are  $D = 2$  and  $D = 3$ , respectively. For the third case, the dimensions of the Kuramoto dynamics associated with both nodes and links are  $D = 3$ . Here, the phases associated with  $i$ th nodes and  $j$ th links are denoted by  $\mathbf{r}_i$  and  $\boldsymbol{\sigma}_j$ , with dimensions  $D_{[0]}$  and  $D_{[1]}$ , respectively. The set of phases on nodes and links are denoted by  $\mathbf{r}$  and  $\boldsymbol{\sigma}$ , respectively. Therefore, for  $N_{[0]}$  nodes,  $\mathbf{r}$  is an  $N_{[0]} \times D_{[0]}$  matrix, while for  $N_{[1]}$  links,  $\boldsymbol{\sigma}$  is an  $N_{[1]} \times D_{[1]}$  matrix.

To describe the effect of the dynamics defined on a  $p$ -dimensional simplex on the dynamics of adjacent simplexes, the algebraic topology can construct the projected dynamics [17]. Here, we discuss the projection of the dynamics of  $\boldsymbol{\sigma}$ . For  $D = 2$ , the dynamics can be expressed as

$$\dot{\boldsymbol{\sigma}} = \tilde{\boldsymbol{\omega}} - \lambda (\mathbf{B}_{[2]} \sin \mathbf{B}_{[2]}^T \boldsymbol{\sigma} - \mathbf{B}_{[1]}^T \sin \mathbf{B}_{[1]} \boldsymbol{\sigma}). \quad (9)$$

Specifically, the projection of the dynamics on nodes are defined as  $\hat{\boldsymbol{\sigma}} = \mathbf{B}_{[1]} \boldsymbol{\sigma}$ . Here,  $\mathbf{B}_{[1]}$  acts as a discrete divergence. Since the incidence matrices satisfy  $\mathbf{B}_{[1]} \mathbf{B}_{[2]} = 0$ , then Eq. (9) becomes

$$\dot{\hat{\boldsymbol{\sigma}}} = \mathbf{B}_{[1]} \tilde{\boldsymbol{\omega}} - \lambda \mathbf{L}_{[0]} \sin(\hat{\boldsymbol{\sigma}}), \quad (10)$$

TABLE I. Three cases of topological signals associated with  $D$ -dimensional Kuramoto dynamics, corresponding to the visual classification shown in Fig. 1(c).

Case	I	II	III
$p = 0$	$D = 2$	$D = 3$	$D = 3$
$\dot{\mathbf{r}}$	$\boldsymbol{\omega} - \lambda_0 \mathbf{B}_{[1]} \sin \mathbf{B}_{[1]}^T \mathbf{r}$	$\mathbf{F} - \lambda_0 (\mathbf{L}_{[0]} \mathbf{r} - \mathbf{I}_N \odot (\mathbf{L}_{[0]} \mathbf{r} \mathbf{r}^T)) \mathbf{r}$	$\mathbf{F} - \lambda_0 (\mathbf{L}_{[0]} \mathbf{r} - \mathbf{I}_N \odot (\mathbf{L}_{[0]} \mathbf{r} \mathbf{r}^T)) \mathbf{r}$
$p = 1$	$D = 2$	$D = 2$	$D = 3$
$\dot{\boldsymbol{\sigma}}$	$\tilde{\boldsymbol{\omega}} - \lambda_1 (\mathbf{B}_{[2]} \sin \mathbf{B}_{[2]}^T \boldsymbol{\sigma} - \mathbf{B}_{[1]}^T \sin \mathbf{B}_{[1]} \boldsymbol{\sigma})$	$\tilde{\boldsymbol{\omega}} - \lambda_1 (\mathbf{B}_{[2]} \sin \mathbf{B}_{[2]}^T \boldsymbol{\sigma} - \mathbf{B}_{[1]}^T \sin \mathbf{B}_{[1]} \boldsymbol{\sigma})$	$\tilde{\mathbf{F}} - \lambda_1 (\mathbf{L}_{[1]} \boldsymbol{\sigma} - \mathbf{I}_N \odot (\mathbf{L}_{[1]} \boldsymbol{\sigma} \boldsymbol{\sigma}^T)) \boldsymbol{\sigma}$

where  $\mathbf{L}_{[0]} = \mathbf{B}_{[1]} \mathbf{B}_{[1]}^T$ . For  $D > 2$ , the dynamics can be expressed as

$$\dot{\boldsymbol{\sigma}} = \tilde{\mathbf{F}} - \lambda (\mathbf{L}_{[1]} \boldsymbol{\sigma} - \mathbf{I}_N \odot (\mathbf{L}_{[1]} \boldsymbol{\sigma} \boldsymbol{\sigma}^T)) \boldsymbol{\sigma}. \quad (11)$$

Since the commutative law does not apply to matrix operations, the projection of  $\boldsymbol{\sigma}$  is not solvable for  $D > 2$ .

By introducing the order parameters as the weight of the coupling strength, coupling between higher-order dynamics is achieved in Millán [17]. Specifically, the control parameter  $\beta_p$  is used as the coefficient of coupling strength, i.e.,  $\lambda \rightarrow \lambda \beta_p$ .  $p$  represents the dimension of the simplex. It has been shown that  $\beta_p$  plays an important role in the emergence of multiple stable states [48–50]. In this paper, we consider three different weights  $\beta_p$ , namely, (a)  $\beta_p = R_q$ , (b)  $\beta_p = R_q^2$ , (c)  $\beta_p = R_p R_q$ . Here,  $R_p$  and  $R_q$  are the order parameters for the dynamics of the  $p$ -dimensional and  $q$ -dimensional simplices, respectively. If  $p = 1$ , then  $q = 0$ , and if  $p = 0$ , then  $q = 1$ . (a) and (b) depict couplings weighted by the order parameters of adjacent order signals, while (c) depicts mixed coupling weighted by the order parameters of its own signal and the adjacent order signals. Since the order parameter depends on the real-time state of the system, the adaptive coupling exists when  $\beta \neq 0$ .

In the next section, the results of numerical simulation will be presented. Unless otherwise specified, the network structure is fully connected and  $\lambda = KN^{-1}$ . The fourth-order Runge Kutta method is used for calculating  $5 \times 10^6$  iterations with  $\Delta t = 10^{-2}$  at each value of  $K$ . After removing an initial transient,  $R_p$  is averaged over  $3 \times 10^5$  iterations for  $N = 2000$  oscillators. We require the elements  $\omega_{k,i}$  of  $\mathbf{W}_i$  and the elements  $\tilde{\omega}_i$  of  $\tilde{\boldsymbol{\omega}}$  follow Gaussian distribution, respectively, i.e.,  $\omega_{k,i} \sim \text{Norm}(0, \delta_0^2)$  and  $\tilde{\omega}_i \sim \text{Norm}(0, \tau^2)$ , with  $k = 1, \dots, D(D-1)/2$  and  $i = 1, \dots, N$ . On a fully connected network,  $\tau = 1/(\delta_1 \sqrt{N-1})$  through properly rescaled [20]. Here,  $\delta_0$  and  $\tau$  are the standard deviations of the Gaussian distribution, which characterize the degree of heterogeneity among the oscillators.

### III. NUMERICAL SIMULATION

In this section, we revealed the roles played by  $\beta_p$  and  $\delta_p$  in phase transitions (Fig. 2). For case I in Table I, the  $D$ -dimensional topological Kuramoto model degenerates to the higher-order Kuramoto model. Here, we first show the results of numerical simulation for case II. The nodal dynamics and the projected dynamics of links are analyzed, namely Eqs. (7) and (10). For all settings of  $\beta_p$ , we discover a discontinuous transition for  $R_0$  from 0 to 0.5 when  $K = 0$ . When  $K > 0$ , the synchronization processes for both  $R_0$  and  $R_1$  exhibit differences in different cases. For  $\beta_p = R_q$ , both  $R_0$  and  $R_1$  generate continuous transitions to synchronization

[Figs. 2(a) and 2(d)]. However,  $R_0$  displays a second discontinuous transitions for  $\beta_p = R_q^2$  [Fig. 2(b)], as well as for  $\beta_p = R_p R_q$  [Fig. 2(c)], when  $\delta_0 = 0.5$ . Meanwhile,  $R_1$  also exhibits a first-order transition when the second transitions occur for  $R_0$ . Therefore,  $\beta_p$  plays a key role in controlling the continuity of phase transition. Notably, when  $\delta_0 = 1.5$ , both  $R_0$  and  $R_1$  depict continuous transitions [Figs. 2(e) and 2(f)], which means that  $\delta_0$  plays another crucial role in switching between continuity and discontinuity of phase transitions.

To reveal the microscopic states of the system before and after the phase transition, the dynamics of the nodes and links are shown in Fig. 3. Taking the phase transition in Fig. 2(c) as an example, 10 individuals are randomly selected for illustration. When there is no coupling between individual dynamics (i.e.,  $K = 0$ ), the order parameters of both the nodes and links are approximately  $R \approx 0$ . The links' dynamics exhibit periodic rotation on the unit circle, while the nodal dynamics rotate on a circular cross section of the unit sphere, with both dynamics displaying incoherent oscillations. When  $K = 2.2$ , the order parameter of the links remains  $R \approx 0$ , whereas the order parameter of the nodes increases to  $R \approx 0.5$ . The links' dynamics still exhibit incoherent oscillations, while the nodal dynamics follow a motion pattern resembling chaos. When  $K = 2.6$ , the order parameters of both the nodes and links

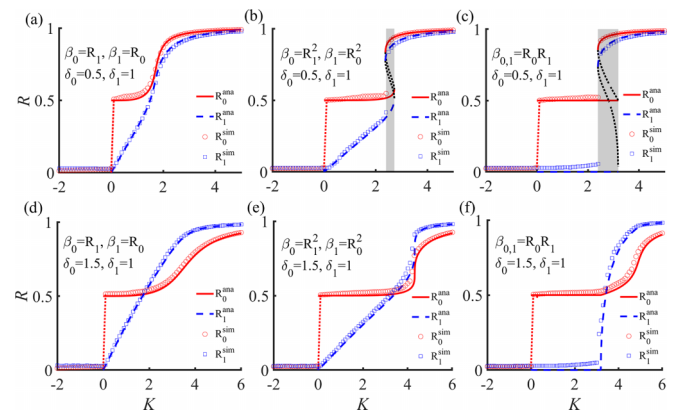


FIG. 2. Numerical simulations and stable theoretical solutions for the evolution of order parameters. Here, 3D Kuramoto model on nodes while 2D Kuramoto model on links.  $\delta_1 = 1$  is fixed for all panels, and  $\delta_0 = 0.5$  is used in the row above (a)–(c), while  $\delta_0 = 1.5$  is used in the row below (d)–(f). The red circles and blue squares respectively depict  $R_0$  and  $R_1$  in numerical simulations. The red-solid curve and blue-chain line correspond to the stable theoretical solutions of  $R_0$  and  $R_1$  from Eqs. (14) and (15), respectively, while the black-dashed line corresponds to the unstable theoretical solutions of  $R_0$  and  $R_1$ .

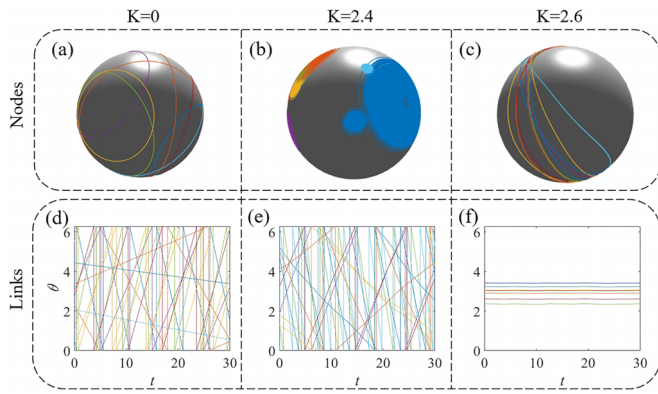


FIG. 3. Microscopic state diagrams before and after the phase transition corresponding to Fig. 2(c). (a)–(c) The motion of node dynamics on the sphere for  $K = 0$ ,  $K = 2.4$ , and  $K = 2.6$ , respectively. (d)–(f) The phase evolution of links’ dynamics for  $K = 0$ ,  $K = 2.4$ , and  $K = 2.6$ , respectively.

approach 1. The links’ dynamics then show weak oscillations, while the nodal dynamics exhibit synchronized rotation on the unit sphere.

We simulated the case of  $D = 3$  in Erdős-Rényi random network (ER network) and scale-free (SF) network. The former characterizes connectivity through to the average degree  $\langle k_i \rangle$ , while the latter has a power-law degree distribution with the exponent  $\gamma$ . We observe that network connectivity significantly influences phase transitions as shown in Fig. 4. Under identical parameter conditions, as the average degree of network decreases, the type of phase transitions shifts from first order to second order. Moreover, an increased network heterogeneity also contributes to smoother synchronization transition curves. Our findings provide a validation for the conclusions drawn in Ling [51].

Figure 5 shows the phase diagram of  $R_0$  for  $D = 3$ . Two scenarios of  $\beta_0$  are studied, which correspond to four phase diagrams of the system in the  $(K, \delta_p)$  plane. Clearly, two

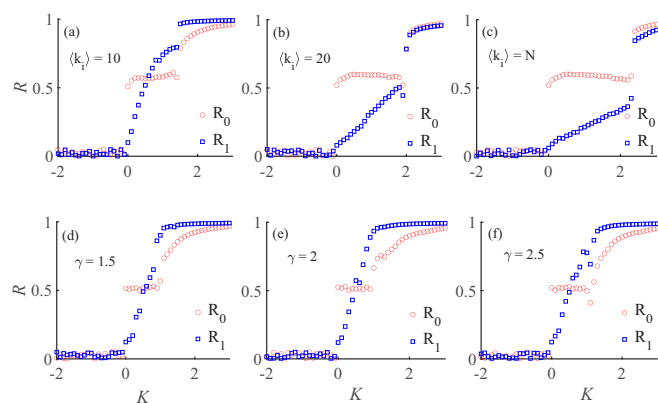


FIG. 4. Phase transitions corresponding to the different network structures. (a)–(c) ER network. (d)–(f) SF network. Here,  $N = 200$ ,  $\delta_1 = 1$ ,  $\delta_0 = 0.5$ . The parameters of network are displayed in the upper left corner of each panel, with the average degree  $\langle k_i \rangle$  corresponding to the ER network, and the exponent  $\gamma$  of degree distribution corresponding to the SF network. Here,  $3D$  Kuramoto model on nodes while  $2D$  Kuramoto model on links.

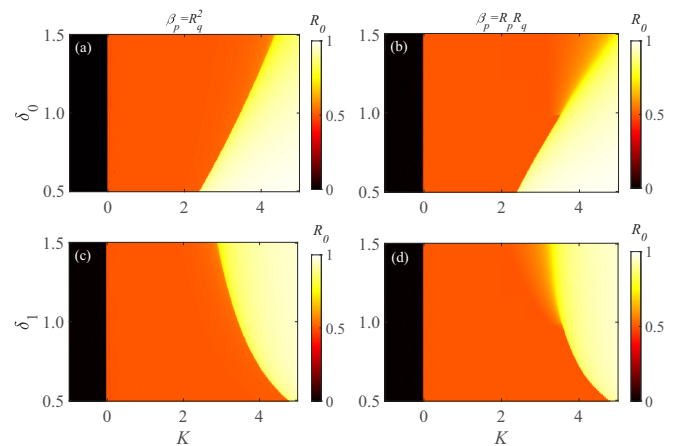


FIG. 5. Phase diagram of  $R_0$  in the  $(K, \delta_p)$  plane. Here,  $3D$  Kuramoto model on nodes while  $2D$  Kuramoto model on links. The upper row represents  $R_0$  for each pair of  $(K, \delta_0)$  when  $\delta_1 = 1$ , which corresponds to the case of (a)  $\beta_p = R_q^2$  and (b)  $\beta_p = R_p R_q$ . The lower row represents  $R_0$  for each pair of  $(K, \delta_1)$  when  $\delta_0 = 1$ , which corresponds to the case of (c)  $\beta_p = R_q^2$  and (d)  $\beta_p = R_p R_q$ .

boundaries between incoherence ( $R \approx 0$ ), and partial coherence ( $R \approx 0.5$ ), as well as the partial coherence state and synchronization ( $R \approx 1$ ), are visible. Additionally, in Fig. 6, we present the results for  $D > 2$  on nodes, while  $D = 2$  on links. For odd  $D$ , i.e.,  $D = 3, 5, 7$ , there are always double first-order phase transitions. For even  $D$ , i.e.,  $D = 2, 4, 6$ , there are always one first-order phase transitions. Meanwhile, we present the case where  $\beta_p = R_p R_q^2$  and find that the width of the hysteresis loop increases with the increase of order for  $\beta_p$ .

For the cases of same dimensional dynamics on nodes and links, namely the  $2D$  Kuramoto model as case I in Table I, and the  $3D$  Kuramoto model as case III in Table I, their results are shown below. The phase diagrams in the  $(K, \delta_p)$  plane for the  $2D$  Kuramoto model as case I in Table I are shown in Fig. 7. Three types of  $\beta_p$  are displayed, namely (a)(d)

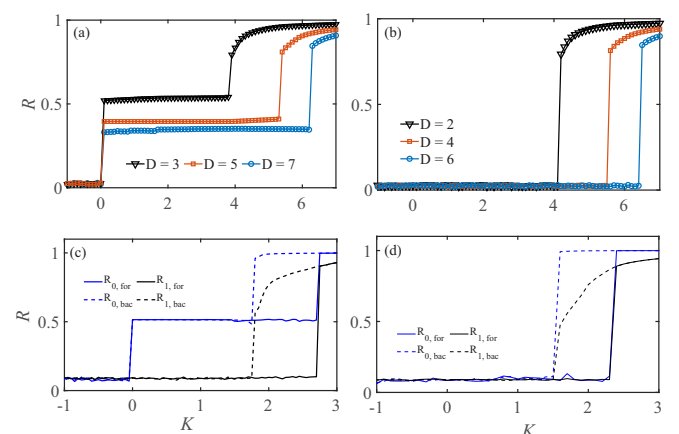


FIG. 6. Phase transitions of the order parameter. Here,  $D > 2$  for nodal dynamics while  $2D$  Kuramoto model on links. (a) Odd  $D$ , i.e.,  $D = 3, 5, 7$ , on nodes (b) Even  $D$ , i.e.,  $D = 2, 4, 6$ , on nodes. (c)  $\beta_p = R_p R_q^2$  for  $D = 3$  and (d)  $\beta_p = R_p R_q^2$  for  $D = 2$ .

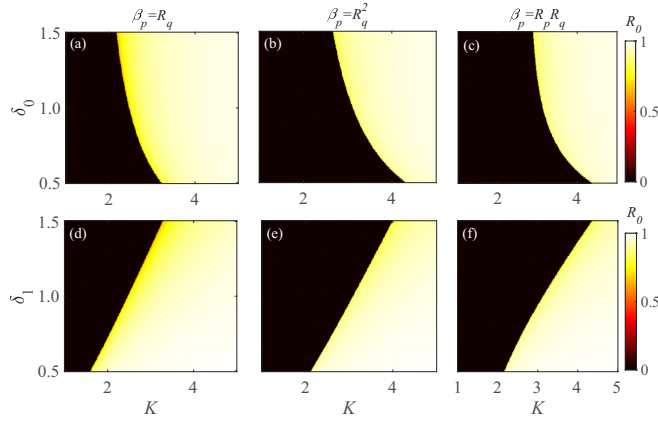


FIG. 7. Phase diagram of  $R_0$  in the  $(K, \delta_p)$  plane for 2D Kuramoto model on both nodes and links. The cases of  $\beta_p = R_q$ ,  $\beta_p = R_q^2$ , and  $\beta_p = R_p R_q$  are displayed in (a)(d), (b)(e), and (c)–(f), respectively.  $\delta_1 = 1$  is in (a)–(c), while  $\delta_0 = 1$  is in (d)–(f).

$\beta_p = R_q$ , (b)(e)  $\beta_p = R_q^2$ , and (c)(f)  $\beta_p = R_p R_q$ . For each case of  $(K, \delta_p)$ , there is always  $\delta_q = 1$ . In all panels,  $R_0$  exhibits discontinuous transitions between incoherence and coherence, while partial coherence does not exist. Phase transitions of the order parameter for 3D Kuramoto model on both nodes and links are shown in Fig. 8. When the 3D Kuramoto model is defined on links, the numerical simulations reveal that it can never be synchronized. In fact, the limitation of 3D models is that they cannot obtain the projection onto nodes.

#### IV. THEORETICAL ANALYSIS

In order to reveal the origin of discontinuous transitions, we provide theoretical analysis of the system described by Eq. (7) for  $D = 3$ . All analyses are based on fully connected networks. The main results are presented below, and more details in the Appendixes. By using the definition of the order parameter, the system can be written as follows:

$$\begin{aligned} \dot{\mathbf{r}}_i &= K\beta_0(\boldsymbol{\rho}_0 - (\boldsymbol{\rho}_0 \cdot \mathbf{r}_i)\mathbf{r}_i) + \boldsymbol{\omega}_i \times \mathbf{r}_i, \\ \dot{\theta}_i &= \hat{\omega}_i + K\beta_1 R_1 \sin \Theta - K\beta_1 \sin \theta_i. \end{aligned} \quad (12)$$

The incoherence of the system at infinite size can be measured by  $R = 0$ , which means that the state  $\mathbf{r}_i$  of each agent

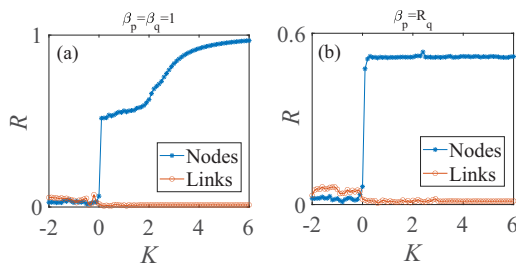


FIG. 8. Phase transitions of the order parameter for 3D Kuramoto model on both nodes and links. (a) The cases of unweighted coupling, i.e.,  $\beta_p = \beta_q = 1$ . (b) The cases of weighted coupling, i.e.,  $\beta_p = R_q$ . Here, the network is the ER network with  $N = 200$  whose average degree is 20.

rotates around their own axes  $\hat{\omega}_i$  with its intrinsic rotation frequency  $\omega_i$ . In Fig. 2,  $R_0$  displays discontinuous transitions from  $R_0 \approx 0$  when  $K = 0$  for all panels, indicating the instability of the incoherent states. We analyze the linear stability of incoherent states, namely introduce a small perturbation to the incoherent solution as  $f = f_0 + \varepsilon e^{st} \xi$ . Here,  $s$  is the characteristic exponent capturing the growth rate of the perturbation. Ultimately, the dispersion relation of  $s$  can be obtained as follows:

$$1 = \frac{2K\beta_0}{9s} + \frac{4K\beta_0 s}{9} \int_0^{+\infty} \frac{g(\omega)}{s^2 + \omega^2} d\omega. \quad (13)$$

In the limit of weak coupling  $K \rightarrow 0^+$ ,  $s \rightarrow 0^+$  along with  $K$ , thus the second term in right-hand sides of Eq. (13) can be ignored. Accordingly, there is  $s = \frac{2}{9}K\beta_0$  from Eq. (13). Here  $\beta_0$  can be regarded as a weighted constant of  $K$ . Since  $s \propto K$ , the incoherent state is stable ( $s < 0$ ) for  $K < 0$ , while it is unstable ( $s > 0$ ) for  $K > 0$ . Obviously, the first discontinuous phase transitions when  $K = 0$  are independent of  $\delta_p$  and  $\beta_p$ . Thus, they occur in all cases shown in Fig. 2.

Next, we analyze the coherence when  $K > 0$ . We are able to derive the self-consistent equation about the order parameter from Eq. (12) in the thermodynamic limit, i.e.,  $N \rightarrow \infty$ . Then an implicit expression regarding  $R_0$  can be yielded as follows:

$$\frac{1}{K\beta_0} = \int_{-1}^1 \int_{-\infty}^{\infty} \Gamma(\zeta, \eta) \frac{h(K\beta_0 R_0 \eta)}{(\sqrt{2\pi} \delta_0)^3} d\eta d\zeta, \quad (14)$$

where  $\Gamma(\zeta, \eta) = \sqrt{\frac{\pi^2}{2}(1 - \eta^2 + \sqrt{(\eta^2 - 1)^2 + 4\eta^2 \zeta^2})}$ , and  $h(x) = x^2 e^{-\frac{x^2}{2\delta_0^2}}$ . A theoretical expression for  $R_1$  can be inferred as follows:

$$R_1 = K\beta_1 \int_{-1}^1 \sqrt{\frac{(1 - \gamma^2)}{2\pi}} \delta_1 e^{-\frac{(K\beta_1 \delta_1 \gamma)^2}{2\delta_0^2}} d\gamma. \quad (15)$$

More details are given in the Appendix C. If  $\delta_0$  and  $\delta_1$  are provided and the specific expression of  $\beta_p$  is given,  $R_0$  and  $R_1$  can be calculated by using numerical methods based on the combination of Eqs. (14) and (15). In Fig. 2, the red-solid curves describe the stable theoretical solutions of  $R_0$ , while the blue-chain line refers to the stable theoretical solutions of  $R_1$ . The black dashed line corresponds to the unstable theoretical solutions of both  $R_0$  and  $R_1$ . As we can see, the bistable states of both  $R_0$  and  $R_1$  only appear in Figs. 2(b) and 2(c), which lead to the second first-order phase transitions in case (b) and (c) when  $K > 0$ . In analogy with the previous study [34], the implicit expression for  $R_0$  for  $D = 2$  is given by

$$\frac{1}{K\beta_0} = \int_{-1}^1 \sqrt{\frac{(1 - \chi^2)}{2\pi \delta_0^2}} e^{-\frac{(K\beta_0 R_0 \chi)^2}{2\delta_0^2}} d\chi. \quad (16)$$

#### V. DISCUSSION

Although extending the Kuramoto model to a high-dimensional space is not a new topic, there has been no research from the perspective of phase transition when it is used as a topological signal. Our study reveals that there are double discontinuous transitions in the three-dimensional Kuramoto model defined on topological signals. For  $D = 3$ , parameters regulating coupling  $\beta_p$ , as well as the natural

frequencies of nodes and edges  $\omega_p$ , are two factors controlling the continuity of phase transitions when  $K > 0$ . They are verified to be related to bistability of order parameters. In addition, there is another first-order phase transition when  $K \rightarrow 0$ , which is proved to exist independently in the three-dimensional Kuramoto model. On the contrary, any coupling controlled by order parameters leads to only one first-order phase transitions for  $D = 2$ . Our study reports a high-dimensional extension of explosive high-order Kuramoto dynamics [17].

When facing large vertebrate predators, collective defense, namely mass stinging responses to perceived threats, forms within these insect communities [52–54]. For instance, honeybees convey the message of aggregation to companions nearby through alarm pheromones. Additionally, some active colloids can form oscillatory clusters through long-range chemical coupling [55], micro-robots and robotic fish utilize infrared, electrical, and acoustic signals for communication [56,57]. We believe that our model is more realistic than previous models for better characterizing swarming and flocking dynamics in high-dimensional space. Recently, some studies have provided progress [58,59]. There are still areas that need to be further explored, such as the addition of higher-order simplexes, the influence of more network structures, and the role of different coupling functions.

ACKNOWLEDGMENTS

This work is supported by the National Natural Science Foundation of China under Grants No. 12275179, and No. 12075089, the National Social Science Fund of China under Grant No. 24CYY098. This work is supported by High Performance Computing Center, University of Shanghai for Science and Technology. We thank Prof. Ginestra Bianconi for discussing with us online and providing valuable suggestions. We also thank Ass. Prof. Jack Murdoch Moore for helpful suggestions. We thank the anonymous reviewers for their comments.

APPENDIX A: A TOY EXAMPLE FOR THE D-DIMENSIONAL TOPOLOGICAL KURAMOTO MODEL

A basic concept is that simplicial complexes represent higher-order networks. A node is a zero-dimensional simplex, a link is a one-dimensional simplex, a triangle is a two-dimensional simplex, a tetrahedron is a three-dimensional simplex, and so on. In Millán [17], by introducing the boundary map in algebraic topology, the incidence matrix  $\mathbf{B}_{[p]}$  describing the topological relationship between  $p$ - and  $(p + 1)$ -dimensional simplices is given.

We present a toy example to describe the  $D$ -dimensional topological Kuramoto model in Fig. 9. In panel (b), we present the construction of the boundary matrix  $\mathbf{B}_{[1]}$ . The  $(i, j)$  en-

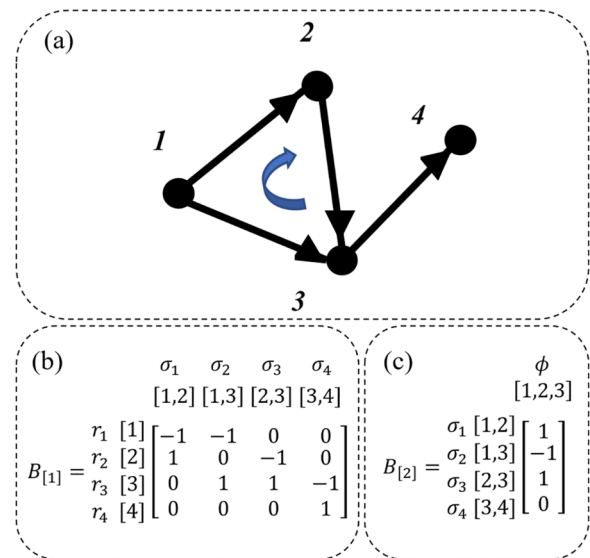


FIG. 9. An example of the high-dimensional oscillators on a simplicial complex. (a) The structure of simplicial complex. (b) Its incidence matrix  $\mathbf{B}_{[1]}$  describing the topological relationship between nodes and links. (c) Its incidence matrix  $\mathbf{B}_{[2]}$  describing the topological relationship between links and triangles.

try of  $\mathbf{B}_{[1]}$  encodes the incidence relationship between the  $i$ th node (zero-dimensional simplex) and the  $j$ th link (one-dimensional simplex). Specifically, if node  $i$  serves as the initial vertex of the oriented link  $j$ , the corresponding entry is  $-1$ ; if node  $i$  is the terminal vertex, the entry is  $1$ . Otherwise, the entry is  $0$ , indicating no incidence between node  $i$  and link  $j$ . In panel (c), we present the construction of the boundary matrix  $\mathbf{B}_{[2]}$ . The  $(i, j)$  entry of  $\mathbf{B}_{[2]}$  encodes the incidence relationship between the  $i$ th link (one-dimensional simplex) and the  $j$ th triangle (two-dimensional simplex). Specifically, if the oriented link  $i$  is aligned with the orientation of the triangle  $j$ , the corresponding entry is  $1$ ; if it is oppositely oriented, the entry is  $-1$ ; if the link does not belong to the boundary of the triangle, the entry is  $0$ . It should be noted that for a rigorous definition of  $\mathbf{B}_{[p]}$  from the perspective of the boundary map, we refer the reader to the study of Millán [17].

According to Eq. (8) in the main text, the zeroth-order Laplace matrix of this toy example is obtained as

$$\mathbf{L}_{[0]} = \begin{bmatrix} 2 & -1 & -1 & 0 \\ -1 & 2 & -1 & 0 \\ -1 & -1 & 3 & -1 \\ 0 & 0 & -1 & 1 \end{bmatrix}. \tag{A1}$$

For  $2D$  Kuramoto model is on nodes, its mathematical expression is

$$\dot{\theta} = \omega - \lambda \mathbf{B}_{[1]} \sin(\mathbf{B}_{[1]}^T \theta) = \begin{bmatrix} \omega_1 + \lambda(\sin(\theta_2 - \theta_1) + \sin(\theta_3 - \theta_1)) \\ \omega_2 + \lambda(\sin(\theta_1 - \theta_2) + \sin(\theta_3 - \theta_2)) \\ \omega_3 + \lambda(\sin(\theta_1 - \theta_3) + \sin(\theta_2 - \theta_3) + \sin(\theta_4 - \theta_3)) \\ \omega_4 + \lambda \sin(\theta_3 - \theta_4) \end{bmatrix}. \tag{A2}$$

For  $D$ -dimensional Kuramoto model is on nodes with  $D > 2$ , and since  $r$  is a row vector, there are  $r_i r_j^T = r_i \cdot r_j$  and  $r_i r_i^T = |r_i|^2 = 1$ , there is

$$\dot{r} = F - \lambda(L_{[0]}r - I_N \odot (L_{[0]}r r^T)r) = \begin{bmatrix} \dot{r}_1 \\ \dot{r}_2 \\ \dot{r}_3 \\ \dot{r}_4 \end{bmatrix} = \begin{bmatrix} W_1 r_1^T + \lambda(r_2 - (r_2 \cdot r_1)r_1 + r_3 - (r_3 \cdot r_1)r_1) \\ W_2 r_2^T + \lambda(r_1 - (r_1 \cdot r_2)r_2 + r_3 - (r_3 \cdot r_2)r_2) \\ W_3 r_3^T + \lambda(r_1 - (r_1 \cdot r_3)r_3 + r_2 - (r_2 \cdot r_3)r_3 + r_4 - (r_4 \cdot r_3)r_3) \\ W_4 r_4^T + \lambda(r_3 - (r_3 \cdot r_4)r_4) \end{bmatrix}. \quad (\text{A3})$$

Clearly, Eq. (A3) is logically consistent with (A2). For the projected dynamics defined on links, according to Eq. (10) in the main text, it can be expressed as

$$\dot{\hat{\sigma}} = \begin{bmatrix} \dot{\hat{\sigma}}_1 \\ \dot{\hat{\sigma}}_2 \\ \dot{\hat{\sigma}}_3 \\ \dot{\hat{\sigma}}_4 \end{bmatrix} = \begin{bmatrix} \hat{\omega}_1 + \lambda(\sin \sigma_2 + \sin \sigma_3 - 2 \sin \sigma_1) \\ \hat{\omega}_2 + \lambda(\sin \sigma_1 + \sin \sigma_3 - 2 \sin \sigma_2) \\ \hat{\omega}_3 + \lambda(\sin \sigma_1 + \sin \sigma_2 + \sin \sigma_4 - 3 \sin \sigma_3) \\ \hat{\omega}_4 + \sin \sigma_3 - \sin \sigma_4 \end{bmatrix}. \quad (\text{A4})$$

Therefore, for this toy model, Eqs. (A3) and (A4) constitute the dynamic equations for numerical simulation.

## APPENDIX B: THE LINEAR STABILITY ANALYSIS OF THE INCOHERENT STATES

Following the approach of Refs. [32,58], the linear stability analysis of incoherent states is derived as follows. As shown in Eq. (5) in the main text, there is

$$\dot{r}_i = K\beta_0(\rho_0 - (\rho_0 \cdot r_i)r_i) + \omega_i \times r_i. \quad (\text{B1})$$

In the limit of infinitely large  $N \rightarrow \infty$ , a density function  $f = f(r, \omega, t)$  is used to describe the macroscopic dynamics of Eq. (B2), which denotes the fraction of agents with the natural rotation  $\omega$  at the position  $r$  in time  $t$ . For  $D = 3$ , there is a continuity equation on the unit sphere,

$$\frac{\partial f}{\partial t} + \frac{1}{\sin \theta} \left( \frac{\partial(f \sin \theta v_\theta)}{\partial \theta} + \frac{\partial(f v_\phi)}{\partial \phi} \right) = 0, \quad (\text{B2})$$

where  $f$  satisfies the normalization condition  $\int_{|r|=1} f(r, \omega, t) dr = 1$ , and  $[v_\theta, v_\phi]$  are given by  $\dot{r} = v_\theta \hat{\theta} + v_\phi \hat{\phi}$  where  $[\hat{\theta}, \hat{\phi}]$  is an orthonormal set of vectors in a 3D space as follows:

$$\begin{aligned} \hat{\theta} &= (\cos \theta \cos \phi, \cos \theta \sin \phi, -\sin \theta)^T, \\ \hat{\phi} &= (-\sin \phi, \cos \phi, 0)^T. \end{aligned} \quad (\text{B3})$$

Thus,  $v_\theta = K\beta_0 \cdot \rho_0 \cdot \hat{\theta} + \omega \cdot \hat{\phi}$  and  $v_\phi = K\beta_0 \cdot \rho_0 \cdot \hat{\phi} - \omega \cdot \hat{\theta}$  can be obtained from Eq. (B1). Introducing the expression of  $v_\theta$  and  $v_\phi$  into Eq. (B2) yields

$$\begin{aligned} \frac{\partial f}{\partial t} - 2f \cdot K\beta_0 \rho \cdot r + \frac{\partial f}{\partial \theta} (K\beta_0 \rho \cdot \hat{\theta} + \omega \cdot \hat{\phi}) \\ + \frac{\partial f}{\partial \phi} \left( \frac{K\beta_0 \rho \cdot \hat{\phi} - \omega \cdot \hat{\theta}}{\sin \theta} \right) = 0. \end{aligned} \quad (\text{B4})$$

The solution of  $f$  for an incoherent state is  $f = f_0 = \frac{1}{4\pi}$ , which corresponds to a state that all the agents are uniformly spread over the surface of the unit sphere for each  $\omega$ . To examine the linear stability of the incoherent state, we

consider a small perturbation to the incoherent solution as  $f = f_0 + \varepsilon e^{st} \xi(\theta, \phi, \omega)$ . In terms of  $f(r, \omega, t)$ , the order parameter  $\rho_0$  defined as the integral form,

$$\begin{aligned} \rho_0 &= \int_{\mathbb{R}^3} \int_{S^2} r f(r, \omega, t) G(\omega) dr d\omega \\ &= \int_{\mathbb{R}^3} \int_0^\pi \int_0^{2\pi} r \varepsilon e^{st} \xi \sin \theta G(\omega) d\omega d\theta d\phi \approx \varepsilon e^{st} \langle \xi \rangle, \end{aligned} \quad (\text{B5})$$

where  $\langle \xi \rangle$  denotes a constant nonzero 3D vector. Substituting  $f$  and  $\rho_0$  into Eq. (B4), and gathering all the linear terms of the first order in  $\varepsilon$ , we get an equation for  $\xi$  as follows:

$$s\xi + \omega_\phi \frac{\partial \xi}{\partial \theta} - \frac{\omega_\theta}{\sin \theta} \frac{\partial \xi}{\partial \phi} = \frac{K\beta_0 \langle \xi \rangle}{2\pi} \cdot r, \quad (\text{B6})$$

In analogy with Ref. [58],  $\xi$  can be derived as follows:

$$\langle \xi \rangle = \frac{2K\beta_0 \langle \xi \rangle}{3} \int_{\mathbb{R}^3} (sI - W)^{-1} G(\omega) d\omega \quad (\text{B7})$$

For a nontrivial solution of  $\langle \xi \rangle$ , there is

$$\det \left( I - \frac{2K\beta_0}{3} \int_{\mathbb{R}^3} (sI - W)^{-1} G(\omega) d\omega \right) = 0, \quad (\text{B8})$$

If the following equation has no root of  $s$  with a positive real part, the perturbation will decay exponentially in time, and the incoherent state is stable. In contrast, the incoherent state loses stability if the real part of one root of  $s$  changes from negative to positive. Finally, the dispersion relation of  $s$  reduces to

$$1 = \frac{2K\beta_0}{9s} + \frac{4K\beta_0 s}{9} \int_0^{+\infty} \frac{g(\omega)}{s^2 + \omega^2} d\omega. \quad (\text{B9})$$

In the limit of weak coupling  $K \rightarrow 0^+$ ,  $s \rightarrow 0^+$  along with  $K$ , thus the second term in right hands of Eq. (B9) can be ignored. Accordingly, there is  $s = \frac{2}{3}K\beta_0$  from Eq. (B9). Here,  $\beta_0$  can be regarded as a weighted constant of  $K$ . Since  $s \propto K$ , the incoherent state is stable ( $s < 0$ ) for  $K < 0$ , while it is unstable ( $s < 0$ ) for  $K > 0$ .

## APPENDIX C: SELF-CONSISTENT ANALYSIS FOR THE ORDER PARAMETERS

Firstly, we aim to provide an analytic prediction of  $R$  for the nodal dynamics with  $K > 0$  in the limit of  $N \rightarrow \infty$ . The nodal dynamics on full-connected network are described as follows:

$$\dot{r}_i = W_i r_i + \lambda \beta_0 \sum_{j=1}^N (r_j - (r_j \cdot r_i)r_i). \quad (\text{C1})$$

For  $D = 3$ , there is  $\mathbf{W}_i \mathbf{r}_i = \boldsymbol{\omega}_i \times \mathbf{r}_i$ . Equation (C1) can be rewritten as follows by using the order parameter, i.e.,  $\boldsymbol{\rho}_0 = \frac{1}{N} \sum_{i=1}^N \mathbf{r}_i$ ,

$$\dot{\mathbf{r}}_i = \boldsymbol{\omega}_i \times \mathbf{r}_i + \lambda \beta_0 N [\boldsymbol{\rho}_0 - (\boldsymbol{\rho}_0 \cdot \mathbf{r}_i) \mathbf{r}_i]. \quad (\text{C2})$$

When the order parameter  $\boldsymbol{\rho}_0$  is at a fixed point, each agent reaches its time asymptotic equilibrium. Thus, the fixed point of these agents are governed by

$$\mathbf{0} = \boldsymbol{\omega}_i \times \mathbf{r}_i^F + \lambda \beta_0 N [\boldsymbol{\rho}_0 - (\boldsymbol{\rho}_0 \cdot \mathbf{r}_i^F) \mathbf{r}_i^F], \quad (\text{C3})$$

where the superscript  $F$  means that the agent is at a fixed point. Note that the above fixed point solution  $\mathbf{r}_i^F$  exists if  $K > 0$ . We define a quantity  $\mu_i = \frac{\omega_i}{\lambda \beta_0 N |\boldsymbol{\rho}_0|}$ , and  $\hat{\boldsymbol{\rho}}_0 = \frac{\boldsymbol{\rho}_0}{|\boldsymbol{\rho}_0|}$ , thus

$$\mathbf{0} = \mu_i (\hat{\boldsymbol{\omega}}_i \times \mathbf{r}_i^F) + (\hat{\boldsymbol{\rho}}_0 - (\hat{\boldsymbol{\rho}}_0 \cdot \mathbf{r}_i^F) \mathbf{r}_i^F). \quad (\text{C4})$$

By equating the square of the norm of Eq. (C4), as well as by dotting Eq. (C4) with  $\hat{\boldsymbol{\omega}}_i$ , there are

$$1 - (\hat{\boldsymbol{\rho}}_0 \cdot \mathbf{r}_i^F)^2 - \mu_i^2 (1 - (\hat{\boldsymbol{\omega}}_i \cdot \mathbf{r}_i^F)^2) = 0, \quad (\text{C5})$$

$$\hat{\boldsymbol{\omega}}_i \cdot \mathbf{r}_i^F - \frac{(\hat{\boldsymbol{\rho}}_0 \cdot \hat{\boldsymbol{\omega}}_i)}{(\hat{\boldsymbol{\rho}}_0 \cdot \mathbf{r}_i^F)} = 0.$$

Furthermore, Eq. (C5) can be derived as

$$(\hat{\boldsymbol{\rho}}_0 \cdot \mathbf{r}_i^F)^4 + (\mu_i^2 - 1) \hat{\boldsymbol{\rho}}_0 \cdot \mathbf{r}_i^F - \mu_i^2 (\hat{\boldsymbol{\rho}}_0 \cdot \hat{\boldsymbol{\omega}}_i)^2 = 0, \quad (\text{C6})$$

which can be solved to obtain

$$\hat{\boldsymbol{\rho}}_0 \cdot \mathbf{r}_i^F = \sqrt{\frac{1 - \mu_i^2 + \sqrt{(\mu_i^2 - 1)^2 + 4\mu_i^2 (\hat{\boldsymbol{\rho}}_0 \cdot \hat{\boldsymbol{\omega}}_i)^2}}{2}}. \quad (\text{C7})$$

In the thermodynamic limit  $N \rightarrow \infty$ ,  $R$  is given by

$$R = \int \hat{\boldsymbol{\rho}}_0 \cdot \mathbf{r}_i^F G(\boldsymbol{\omega}) d\boldsymbol{\omega}, \quad (\text{C8})$$

and in analogy with Refs. [32,58], for  $\boldsymbol{\omega} \sim N(0, \delta_1^2)$ , and  $G(\boldsymbol{\omega}) = g(\omega)U(\hat{\boldsymbol{\omega}})$  are substituted into Eq. (C8),

$$1 = \lambda \beta_0 N \int_{-1}^1 \int_{-\infty}^{\infty} G(\zeta, \eta) \frac{h(\lambda \beta_0 N R \eta)}{(\sqrt{2\pi} \delta_1)^3} d\eta d\zeta, \quad (\text{C9})$$

where  $G(\zeta, \eta) = \sqrt{\frac{\pi^2}{2} (1 - \eta^2 + \sqrt{(\eta^2 - 1)^2 + 4\eta^2 \zeta^2})}$ ,  $h(x) = x^2 e^{-\frac{x^2}{2\delta_1^2}}$  and  $\lambda = KN^{-1}$ .

For  $D = 2$ , Eq. (4) can be simplified as

$$\dot{\theta} = \omega_i + \lambda \beta_0 \sum_{j=1}^N \sin(\theta_j - \theta_i), \quad (\text{C10})$$

and following the classical analysis given in Ref. [34], then

$$\frac{1}{\lambda \beta_0 N} = \int_{-1}^1 \sqrt{\frac{(1 - \chi^2)}{2\pi \delta_0^2}} e^{-\frac{(\lambda \beta_0 N R_0 \chi)^2}{2\delta_0^2}} d\chi. \quad (\text{C11})$$

Next, we will focus on the edge dynamics, which are described as follows:

$$\dot{\theta}^{[-1]} = \omega^{[-1]} - \lambda \beta_1 L_{[0]} \sin \theta^{[-1]}, \quad (\text{C12})$$

with  $\omega^{[-1]} = \mathbf{B}_{[1]} \tilde{\omega}$ . For convenience, the network is considered fully connected, and the superscript  $[-]$  is hidden. We introduce the definition of order parameter,

$$R_1 e^{i\Phi} = N^{-1} \sum_{j=1}^N e^{i\theta_j}. \quad (\text{C13})$$

Accordingly, Eq. (C12) can be rewritten as

$$\dot{\theta} = \tilde{\omega} + \lambda \beta_1 N R_1 \sin \Phi - \lambda N \sin \theta. \quad (\text{C14})$$

In the limit of infinitely large  $N \rightarrow \infty$ , the macroscopic dynamics of the system conveniently described by a density function  $f(\theta, \tilde{\omega}, t)$ , which denotes the fraction of oscillators with the natural frequency  $\tilde{\omega}$  at the position  $\theta$  in time  $t$ . There is the normalization condition

$$\int_0^{2\pi} f_\theta d\theta = 1, \quad (\text{C15})$$

and the continuity equation

$$\frac{\partial f_\theta}{\partial t} + \frac{\partial f_\theta v_\theta}{\partial \theta} = 0 \quad (\text{C16})$$

with the velocity  $v_\theta$  given by  $\dot{\theta}$ , i.e., Eq. (C14). Accordingly, the complex order parameters are given by

$$\rho_1 = R_1 e^{i\Phi} = N^{-1} \int f_\phi e^{i\phi} d\phi, \quad (\text{C17})$$

and  $f_\phi$  can be expressed as by Fourier expansion

$$f_\phi = 2\pi^{-1} \left( 1 + \sum_{m=1}^{\infty} \tilde{f}_m e^{im\phi} + \text{c.c.} \right). \quad (\text{C18})$$

We follow Ott-Antonsen ansatz to solve this continuity equation, and  $\tilde{f}_m = \alpha^m$ , where  $\alpha$  is given by

$$\frac{\partial \alpha}{\partial t} + i\alpha (\tilde{\omega} + \lambda \beta_1 N R_1 \sin \Phi) + \frac{\lambda \beta_1 N}{2} (\alpha^2 - 1) = 0. \quad (\text{C19})$$

Since the average value of  $\dot{\phi}$  is zero, the nonrotating stationary solutions of the above equation for  $\alpha$  is  $\partial_t \alpha = 0$ . Thus, there is

$$\alpha = -i \left( \frac{\tilde{\omega}}{\lambda \beta_1 N} + R_1 \sin \Phi \right) \pm \sqrt{1 - \left( \frac{\tilde{\omega}}{\lambda \beta_1 N} + R_1 \sin \Phi \right)^2}. \quad (\text{C20})$$

By inserting this expression into the expression of  $\rho_1$ , we get the following expression:

$$R_1 \sin \Phi = \int_{\left| \frac{\tilde{\omega}}{\lambda \beta_1 N} + R_1 \sin \Phi \right| \leq 1} \sqrt{1 - \left( \frac{\tilde{\omega}}{\lambda \beta_1 N} + R_1 \sin \Phi \right)^2} \times G(\tilde{\omega}) d\tilde{\omega}. \quad (\text{C21})$$

We define  $\mu = \frac{\tilde{\omega}}{\lambda \beta_1}$ , and  $G(\tilde{\omega}) = \sqrt{\frac{\delta_2}{2\pi}} e^{-\frac{\delta_2 (\lambda \beta_1 N \mu)^2}{2}}$ , then there is

$$R_1 = \lambda \beta_1 N \int_{-1}^1 \sqrt{\frac{(1 - \mu^2)}{2\pi}} \delta_2 e^{-\frac{(\lambda \beta_1 N \delta_2 \mu)^2}{2}} d\mu. \quad (\text{C22})$$

- [1] A. Ziepeke, I. Maryshev, I. S. Aranson, and E. Frey, Multi-scale organization in communicating active matter, *Nat. Commun.* **13**, 6727 (2022).
- [2] A. Sokolov, I. S. Aranson, J. O. Kessler, and R. E. Goldstein, Concentration dependence of the collective dynamics of swimming bacteria, *Phys. Rev. Lett.* **98**, 158102 (2007).
- [3] E. Lauga and T. R. Powers, The hydrodynamics of swimming microorganisms, *Rep. Prog. Phys.* **72**, 096601 (2009).
- [4] I. D. Couzin and J. Krause, Self-organization and collective behavior in vertebrates, *Adv. Study Behav.* **32**, 1 (2003).
- [5] D. Gorbonos, R. Ianculescu, J. G. Puckett, R. Ni, N. T. Ouellette, and N. S. Gov, Long-range acoustic interactions in insect swarms: An adaptive gravity model, *New J. Phys.* **18**, 073042 (2016).
- [6] C. Chen, S. Liu, X. Shi, H. Chaté, and Y. Wu, Weak synchronization and large-scale collective oscillation in dense bacterial suspensions, *Nature (London)* **542**, 210 (2017).
- [7] A. Araque, G. Carmignoto, P. G. Haydon, S. H. R. Oliet, R. Robitaille, and A. Volterra, Gliotransmitters travel in time and space, *Neuron* **81**, 728 (2014).
- [8] D. Attwell, A. M. Buchan, S. Charpak, M. Lauritzen, B. A. MacVicar, and E. A. Newman, Glial and neuronal control of brain blood flow, *Nature (London)* **468**, 232 (2010).
- [9] K. Kisler, A. R. Nelson, A. Montagne, and B. V. Zlokovic, Cerebral blood flow regulation and neurovascular dysfunction in Alzheimer disease, *Nat. Rev. Neurosci.* **18**, 419 (2017).
- [10] K. Alim, G. Anselem, F. Peaudecerf, M. P. Brenner, and A. Pringle, Random network peristalsis in *Physarum polycephalum* organizes fluid flows across an individual, *Proc. Natl. Acad. Sci. USA* **110**, 13306 (2013).
- [11] A. T. Winder, C. Echagarruga, Q. Zhang, and P. J. Drew, Weak correlations between hemodynamic signals and ongoing neural activity during the resting state, *Nat. Neurosci.* **20**, 1761 (2017).
- [12] J. W. Rocks, A. J. Liu, and E. Katifori, Hidden topological structure of flow network functionality, *Phys. Rev. Lett.* **126**, 028102 (2021).
- [13] G. Manzano, F. Galve, G. L. Giorgi, E. Hernández-García, and R. Zambrini, Synchronization, quantum correlations and entanglement in oscillator networks, *Sci. Rep.* **3**, 1439 (2013).
- [14] D. Witthaut, S. Wimberger, R. Burioni, and M. Timme, Classical synchronization indicates persistent entanglement in isolated quantum systems, *Nat. Commun.* **8**, 14829 (2017).
- [15] A. Y. Kitaev, Fault-tolerant quantum computation by anyons, *Ann. Phys.* **303**, 2 (2003).
- [16] G. Semeghini, H. Levine, A. Keesling, S. Ebadi, T. T. Wang, D. Bluvstein, R. Verresen, H. Pichler, M. Kalinowski, R. Samajdar *et al.*, Probing topological spin liquids on a programmable quantum simulator, *Science* **374**, 1242 (2021).
- [17] A. P. Millán, J. J. Torres, and G. Bianconi, Explosive higher-order Kuramoto dynamics on simplicial complexes, *Phys. Rev. Lett.* **124**, 218301 (2020).
- [18] S. Barbarossa and S. Sardellitti, Topological signal processing over simplicial complexes, *IEEE Trans. Signal Process.* **68**, 2992 (2020).
- [19] M. T. Schaub, Y. Zhu, J. Seby, T. M. Roddenberry, and S. Segarra, Signal processing on higher-order networks: Livin' on the edge... and beyond, *Signal Process.* **187**, 108149 (2021).
- [20] R. Ghorbanchian, J. G. Restrepo, J. J. Torres, and G. Bianconi, Higher-order simplicial synchronization of coupled topological signals, *Commun. Phys.* **4**, 120 (2021).
- [21] S. Sardellitti and S. Barbarossa, Topological signal processing over generalized cell complexes, *IEEE Trans. Signal Process.* **72**, 687 (2024).
- [22] K. Li, T. Shi, and X. Li, Synchronization of topological signals on simplicial complexes with higher-dimensional simplices, *IEEE Trans. Network Sci. Eng.* **11**, 1124 (2024).
- [23] L. Giambagli, L. Calmon, R. Muolo, T. Carletti, and G. Bianconi, Diffusion-driven instability of topological signals coupled by the Dirac operator, *Phys. Rev. E* **106**, 064314 (2022).
- [24] S. Krishnagopal and G. Bianconi, Topology and dynamics of higher-order multiplex networks, *Chaos, Solitons Fractals* **177**, 114296 (2023).
- [25] L. Calmon, J. G. Restrepo, J. J. Torres, and G. Bianconi, Dirac synchronization is rhythmic and explosive, *Commun. Phys.* **5**, 253 (2022).
- [26] L. Calmon, S. Krishnagopal, and G. Bianconi, Local Dirac synchronization on networks, *Chaos* **33**, 033117 (2023).
- [27] L. Calmon, M. T. Schaub, and G. Bianconi, Dirac signal processing of higher-order topological signals, *New J. Phys.* **25**, 093013 (2023).
- [28] T. Carletti, L. Giambagli, and G. Bianconi, Global topological synchronization on simplicial and cell complexes, *Phys. Rev. Lett.* **130**, 187401 (2023).
- [29] J. A. Acebrón, L. L. Bonilla, C. J. P. Vicente, F. Ritort, and R. Spigler, The Kuramoto model: A simple paradigm for synchronization phenomena, *Rev. Mod. Phys.* **77**, 137 (2005).
- [30] K. Kovalenko, X. Dai, K. Alfaro-Bittner, A. M. Raigorodskii, M. Perc, and S. Boccaletti, Contrarians synchronize beyond the limit of pairwise interactions, *Phys. Rev. Lett.* **127**, 258301 (2021).
- [31] V. Capraro and M. Perc, Mathematical foundations of moral preferences, *J. R. Soc. Interface* **18**, 20200880 (2021).
- [32] S. Chandra, M. Girvan, and E. Ott, Continuous versus discontinuous transitions in the  $D$ -dimensional generalized Kuramoto model: Odd  $D$  is different, *Phys. Rev. X* **9**, 011002 (2019).
- [33] R. Olfati-Saber, Swarms on sphere: A programmable swarm with synchronous behaviors like oscillator networks, In *Proceedings of the 45th IEEE Conference on Decision and Control* (IEEE, San Diego, CA, 2006), pp. 5060–5066.
- [34] X. Dai, X. Li, H. Guo, D. Jia, M. Perc, P. Manshour, Z. Wang, and S. Boccaletti, Discontinuous transitions and rhythmic states in the  $D$ -dimensional Kuramoto model induced by a positive feedback with the global order parameter, *Phys. Rev. Lett.* **125**, 194101 (2020).
- [35] X. Dai, K. Kovalenko, M. Molodyk, Z. Wang, X. Li, D. Musatov, A. M. Raigorodskii, K. Alfaro-Bittner, G. D. Cooper, G. Bianconi, and S. Boccaletti,  $D$ -dimensional oscillators in simplicial structures: Odd and even dimensions display different synchronization scenarios, *Chaos, Solitons Fractals* **146**, 110888 (2021).
- [36] M. A. M. de Aguiar, Generalized frustration in the multidimensional Kuramoto model, *Phys. Rev. E* **107**, 044205 (2023).
- [37] W. Zou, S. He, D. V. Senthilkumar, and J. Kurths, Solvable dynamics of coupled high-dimensional generalized limit-cycle oscillators, *Phys. Rev. Lett.* **130**, 107202 (2023).
- [38] S. Lee, Y. Jeong, S. Son, and K. Krischer, Volcano transition in a system of generalized Kuramoto oscillators with random

- frustrated interactions, *J. Phys. A: Math. Theor.* **57**, 085702 (2024).
- [39] A. Yadav, Krishnanand J, V. K. Chandrasekar, W. Zou, J. Kurths, and D. V. Senthilkumar, Exotic swarming dynamics of high-dimensional swarmalators, *Phys. Rev. E* **109**, 044212 (2024).
- [40] R. Fariello and M. A. M. de Aguiar, Exploring the phase diagrams of multidimensional Kuramoto models, *Chaos, Solitons Fractals* **179**, 114431 (2024).
- [41] A. Crnkíć and V. Jaćimović, Swarms on the 3-sphere with adaptive synapses: Hebbian and anti-Hebbian learning rule, *Syst. Control Lett.* **122**, 32 (2018).
- [42] A. Crnkíć and V. Jaćimović, Chimeras and traveling waves in ensembles of Kuramoto oscillators off the Poisson manifold, *Chaos* **34**, 023130 (2024).
- [43] C. Zheng, R. Toenjes, and A. Pikovsky, Transition to synchrony in a three-dimensional swarming model with helical trajectories, *Phys. Rev. E* **104**, 014216 (2021).
- [44] F. Ritort, Solvable dynamics in a system of interacting random tops, *Phys. Rev. Lett.* **80**, 6 (1998).
- [45] J. R. Blake and M. A. Sleight, Mechanics of ciliary locomotion, *Biol. Rev.* **49**, 85 (1974).
- [46] N. Hirokawa, Y. Tanaka, Y. Okada, and S. Takeda, Nodal flow and the generation of left-right asymmetry, *Cell* **125**, 33 (2006).
- [47] T. Niedermayer, B. Eckhardt, and P. Lenz, Synchronization, phase locking, and metachronal wave formation in ciliary chains, *Chaos* **18**, 037128 (2008).
- [48] G. Filatrella, N. F. Pedersen, and K. Wiesenfeld, Generalized coupling in the Kuramoto model, *Phys. Rev. E* **75**, 017201 (2007).
- [49] X. Zhang, S. Boccaletti, S. Guan, and Z. Liu, Explosive synchronization in adaptive and multilayer networks, *Phys. Rev. Lett.* **114**, 038701 (2015).
- [50] W. Zou and J. Wang, Dynamics of the generalized Kuramoto model with nonlinear coupling: Bifurcation and stability, *Phys. Rev. E* **102**, 012219 (2020).
- [51] X. Ling, W. Ju, N. Guo, K. Zhu, C. Wu, and Q. Hao, Effects of topological characteristics on rhythmic states of the D-dimensional Kuramoto model in complex networks, *Chaos* **32**, 013118 (2022).
- [52] D. M. T. Nguyen, M. L. Iuzzolino, A. Mankel, K. Bozek, G. J. Stephens, and O. Peleg, Flow-mediated olfactory communication in honeybee swarms, *Proc. Natl. Acad. Sci. USA* **118**, e2011916118 (2021).
- [53] S. Ganga Prasath and L. Mahadevan, Rheomergy: Collective behaviour mediated by active flow-based recruitment, *Proc. R. Soc. A* **479**, 20220470 (2023).
- [54] A. López-Incera, M. Nouvian, K. Ried, T. Müller, and H. J. Briegel, Honeybee communication during collective defence is shaped by predation, *BMC Biol.* **19**, 106 (2021).
- [55] A. Altemose, M. A. Sánchez-Farrán, W. Duan, S. Schulz, A. Borhan, V. H. Crespi, and A. Sen, Chemically controlled spatiotemporal oscillations of colloidal assemblies, *Angew. Chem. Int. Ed.* **56**, 7817 (2017).
- [56] S. Li, R. Batra, D. Brown, H. Chang, N. Ranganathan, C. Hoberman, D. Rus, and H. Lipson, Particle robotics based on statistical mechanics of loosely coupled components, *Nature (London)* **567**, 361 (2019).
- [57] H. Xie, M. Sun, X. Fan, Z. Lin, W. Chen, L. Wang, L. Dong, and Q. He, Reconfigurable magnetic microrobot swarm: Multimode transformation, locomotion, and manipulation, *Sci. Robot.* **4**, eaav8006 (2019).
- [58] W. Zou, Solvable dynamics of the three-dimensional Kuramoto model with frequency-weighted coupling, *Phys. Rev. E* **109**, 034215 (2024).
- [59] J. Wang, C. Gu, and W. Zou, Rhythmic states and first-order phase transitions in adaptive coupled three-dimensional limit-cycle oscillators, *Phys. Rev. E* **110**, 044209 (2024).